Journal of Molecular Catalysis A: Chemical 336 (2011) 58–63

Contents lists available at ScienceDirect

Journal of Molecular Catalysis A: Chemical

journal homepage: www.elsevier.com/locate/molcata

Influence of neodymium ions on photocatalytic activity of TiO_2 synthesized by sol–gel and precipitation methods

T.L.R. Hewer[a], E.C.C. Souza[b], T.S. Martins[c], E.N.S. Muccillo[b], R.S. Freire[a,*]

[a] Instítuto de Química, Universidade de São Paulo-USP, C.P. 26077, CEP 05513-000, São Paulo, Brazil
[b] Instituto de Pesquisas Energéticas e Nucleares-IPEN, C.P. 11049, CEP 05422-970, São Paulo, Brazil
[c] Departamento de Ciências Exatas e da Terra,Universidade Federal de São Paulo-UNIFESP, CEP 09972-270, São Paulo, Brazil

ARTICLE INFO

Article history:
Received 1 April 2010
Received in revised form 7 December 2010
Accepted 17 December 2010
Available online 24 December 2010

Keywords:
Heterogeneous photocatalysis
TiO_2 nanoparticle
Composite
Doping

ABSTRACT

Titanium dioxide with and without the addition of neodymium ions was prepared using sol–gel and precipitation methods. The resulting catalysts were characterized by thermal analysis, X-ray diffraction and BET specific surface area. Neodymium addition exerted a remarkable influence on the phase transition temperature and the surface properties of the TiO_2 matrix. TiO_2 samples synthesized by precipitation exhibit an exothermic event related from the amorphous to anatase phase transition at 510 °C, whereas in Nd-doped TiO_2 this transition occurred at 527 °C. A similar effect was observed in samples obtained using sol–gel method. The photocatalytic reactivity of the catalysts was evaluated by photodegradation of Remazol Black B (RB) under ultraviolet irradiation. Nd-doped TiO_2 showed enhanced photodegradation ability compared to undoped TiO_2 samples, independent of the method of synthesis. In samples obtained by sol–gel, RB decoloration was enhanced by 16% for TiO_2 doped with 0.5% neodymium ions.

1. Introduction

The advanced oxidation processes (AOP) are becoming more important in the area of wastewater treatment, since these processes result in efficient degradation and mineralization of toxic organic compounds that are resistant to traditional treatments such as biological processes [1]. They rely mainly on the formation of reactive and short-lived oxygen-containing intermediates such as hydroxyl radicals (•OH) [2]. The hydroxyl radical is a powerful oxidant and a short lived, highly reactive, non-selective reagent [2,3].

Heterogeneous photocatalysis is included in the class of processes which produce hydroxyl radicals. Semiconductors (e.g., TiO_2, Fe_2O_3, CdS and ZnO) can act as sensitizers for light-induced redox processes due to their electronic structure, which is characterized by a filled valence band and an empty conduction band. When a photon with energy $h\nu$ matches or exceeds the bandgap energy, E_g, of the semiconductor, an electron, e_{cb}^-, is promoted from the valence band, VB, into the conduction band, CB, leaving behind a hole, h_{vb}^+. Excited state conduction-band electrons and valence-band holes can recombine and dissipate the input energy as heat, get trapped in metastable surface states, or react with electron donors and electron acceptors adsorbed on the semiconductor surface [4]. The pair e_{cb}^-/h_{vb}^+ photogenerated in the semiconductor, in contact with O_2 or H_2O and OH^- adsorbed in its surface, leads to the formation of radical species.

TiO_2 is by far the most useful material for photocatalytic purposes, due to its electronic properties, chemical stability, non-toxicity and low cost [3–7]. Titanium dioxide exists in three main crystallographic forms, anatase, rutile and brookite; in most cases, anatase has been found to be photocatalytically more active than the others [8]. In the literature, several preparation methods of TiO_2 in the form of powder, crystals or thin films have been proposed. The precipitation method involves precipitation of hydroxides by the addition of a basic solution (NH_4OH, NaOH and urea) to raw material, followed by calcinations to crystallize the oxide [9]. Sol–gel methods are normally used to form powder, thin films and membranes. There are many advantages of the sol–gel and precipitation methods such as homogeneity, flexibility in introducing dopants in large concentration, stoichiometry control and processing ease [10–12].

There are still basic problems to be solved to improve the photocatalytic activities of TiO_2. Because TiO_2 has a high band gap energy (E_g), it is excited mainly by UV light (for the anatase allotrope form $E_g = 3.2$ eV and $\lambda_g < 384$ nm). Thus, this practically precludes the use of sunlight or visible light as irradiation sources. Moreover, the high rate of electron–hole recombination on TiO_2 particles results in a low efficiency of photocatalysis [13].

Doping methods have been applied for modifying the electronic structure of TiO_2 nanoparticles, in order to improve catalytic activities. Dopants can be segregated on the TiO_2 nanostructure surface

* Corresponding author at: Instituto de Química, USP, Departamento de Química Fundamental, Av Prof Lineu Prestes 748, 05508-000 São Paulo, Brazil.
Tel.: +55 11 3091 1495; fax: +55 11 3091 1495.
E-mail address: rsfreire@iq.usp.br (R.S. Freire).

1381-1169/$ – see front matter © 2010 Elsevier B.V. All rights reserved.
doi:10.1016/j.molcata.2010.12.010

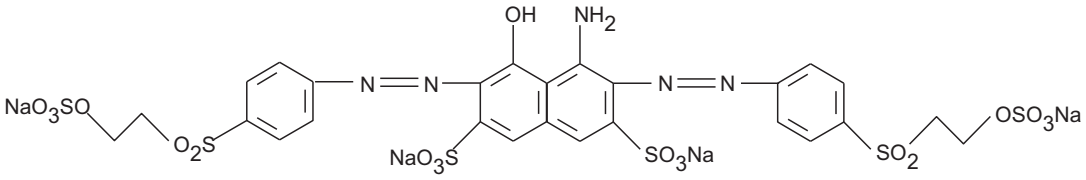

Scheme 1. Structure of the dye Remazol Black B.

or they can be incorporated into the lattice [14]. Different dopants do not have the same effect on the interaction with electrons and/or holes, due to the different position of the dopants in the host lattice. The coordination environments of the dopants are influenced not only by the nature of the dopants, such as ionic radii and concentration, but also by the synthesis method [15]. Lanthanide ions are known for their ability to form complexes with various Lewis bases (e.g., amines, aldehydes, thiols, etc.) via interactions of functional groups of the base with lanthanide f-orbitals. Thus, incorporation of lanthanide ions in a TiO_2 matrix could provide a means to concentrate the organic pollutant at the semiconductor surface, extend the photocatalytic response to visible region and improve the separation efficiency of photo-induced electron–hole pairs of titânia [16–19].

Neodymium is one of the lanthanide ions that can be employed to improve the photoactivity of TiO_2. Xu et al. [20] prepared a series of Nd–TiO_2 nanotubes by sol–gel method and hydrothermal treatment. The photocatalytic activity of TiO_2 nanotubes pure and doped was evaluated in the degradation of methyl orange dye. The nanotubes containing 0.3% of Nd had a better photocatalytic response compared to pure TiO_2. Shahamoradi et al. [21] prepared TiO_2 nanoparticles doped with Nd by hydrothermal method. The effect of neodymium on the photocatalytic activity of TiO_2 was evaluated in the degradation of municipal wastewater. All materials containing Nd showed better photocatalytic response compared to pure TiO_2. The photocatalyst containing 5% neodymium degraded up to 95% of the wastewater. Wang et al. [22] evaluated the effects of Nd content on the physical structure and photocatalytic activities of doped titania hollow sphere samples, it is found that the optimal Nd-doped concentration was 3.9%.

This work reports the degradation of the azo dye Remazol Black B (RB) by Nd-doped TiO_2. Non-doped and doped TiO_2 were prepared using the sol–gel and precipitation methods, thus allowing for evaluation of the effects of neodymium ions on the surface characteristics and on the photocatalytic properties of TiO_2.

2. Experimental

2.1. Preparation of pure and Nd doped TiO_2 nanoparticles

Nominally pure TiO_2 and neodymium-doped TiO_2 were prepared by sol–gel and precipitation routes. The procedure for the preparation of these catalysts had been reported previously [23,24]. The concentration of neodymium ions in the titania matrix was 0.5 wt%. The sol–gel route started from titanium isopropoxide (Gelest) and hydrated neodymium chloride (99.9% Aldrich). The appropriate amount of $NdCl_3{\cdot}7H_2O$ was dissolved in propanol and mixed with 13 mL titanium isopropoxide. The titanium–neodymium solution was then added dropwise under vigorous stirring to 200 mL of an aqueous nitric acid solution. Stirring was maintained until a transparent solution was obtained. The transparent sols were dried at 70 °C and calcinated under air at 580 °C for 1 h. Undoped TiO_2 was synthesized using an identical method. The titanium precursor in the precipitation route was titanium chloride ($TiCl_4$, Aldrich). An appropriate amount of neodymium chloride dissolved in distilled water was added to a $TiCl_4$ solution. The Nd/Ti^{4+} mixture was slowly added to 100 mL of a solution of NH_4Cl at pH 10. The resulting $Nd(OH)_3/Ti(OH)_4$ precipitate was washed twice with water and subsequently washed with n-propanol and n-butanol, dried at 70 °C and calcinated in air at 580 °C for 1 h. All products were kept in desiccators under $CaCl_2$ prior to use.

2.2. Characterization

X-ray diffractograms of the calcinated samples were recorded using a Philips powder diffractometer. The diffraction patterns were recorded at room temperature using Ni-filtered CuK_α radiation ($\lambda = 1.5418$ Å). The percentage of anatase can be estimated from the respective integrated XRD peak intensities using the following equation [25]: $X(\%) = 100/(1 + 1.265 I_R/I_A)$, where I_A represents the intensity of the anatase peak at $2\theta = 25.3^\circ$ and I_R is that of the rutile peak at $2\theta = 27.9^\circ$. X is the weight percent of anatase phase in the sample.

Nitrogen adsorption measurements were carried out at −196 °C using a Micromeritics Model ASAP 2010 Volumetric Adsorption Analyzer. The surface area was determined according to the standard Brunauer, Emmet and Teller (BET) method. The particle size was calculated using the following equation: $D_{BET} = 6000/\rho S$; where D_{BET} is the average nanoparticles size (nm), ρ is the powder density ($g\,cm^{-3}$) and S is the specific surface area ($m^2\,g^{-1}$) measured via the BET method.

Thermogravimetric/derivative thermogravimetric (TG/DTG) curves were obtained with a Shimadzu TGA-50 thermobalance in a temperature range 25–800 °C, using a platinum crucible, approximately 1.5 mg of the sample, dynamic air atmosphere ($50\,mL\,min^{-1}$) and a heating rate of $10\,°C\,min^{-1}$. Differential scanning calorimetry (DSC) curves were obtained on a Shimadzu DSC-50 cell using partially closed aluminum crucibles with ca. 1.5 mg samples, under dynamic nitrogen atmosphere ($100\,mL\,min^{-1}$) in a temperature range 25–600 °C and with the same heating rates used for TG. The DSC cell was calibrated with indium (mp 156.6 °C and $\Delta H_{fusion} = 28.54\,J\,g^{-1}$) and zinc (mp 419.6 °C).

2.3. Evaluation of the photocatalytic activity

Black Remazol B (DyStar Company), Scheme 1, was chosen as model dye to perform the catalysis tests. This commercial dye was used as received without any further purification step.

Experiments were performed in an open batch system. The system consisted of a $400\,cm^{-3}$ glass cylindrical reactor that housed the dye solutions, a water cooling jacket to keep the reactor content at constant temperature (20 °C), a mechanical stirrer to keep the photocatalyst powder suspended (stirring rate: 500 rpm) and a gas disperser to bubble the solution with a stream ($15\,L\,h^{-1}$) of oxygen. The photocatalytic investigation was performed using 300 mL of 250 mg L^{-1} RB aqueous solutions and 150 mg of the respective photocatalyst. The suspension was kept in the dark for 40 min. After this adsorption step the suspension was irradiated with a 125 W high pressure mercury lamp (Philips), which provided UV-A light intensity of $2.2\,mW\,cm^{-2}$. At convenient intervals, samples were

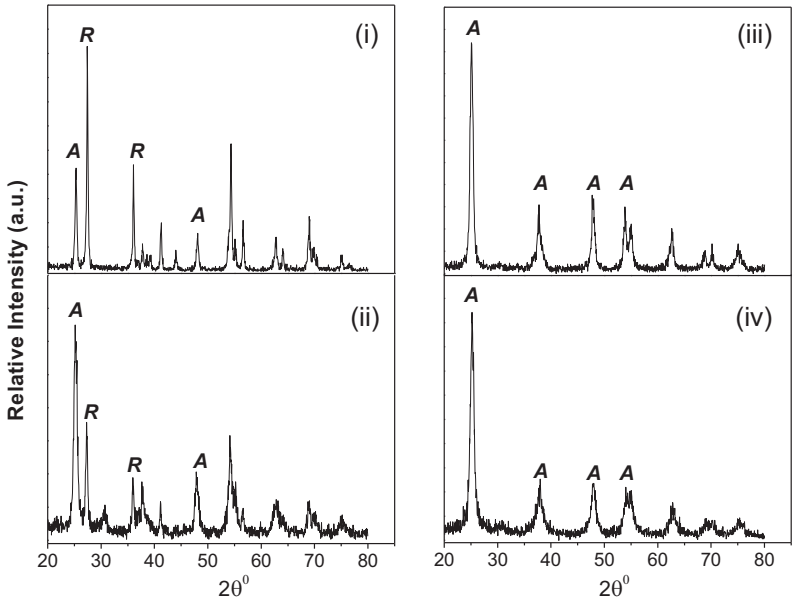

Fig. 1. XRD patterns of the different samples. Synthesized by sol–gel: undoped TiO_2 (i) and TiO_2 doped with 0.5 wt % Nd. (ii) Synthesized by precipitation: undoped TiO_2 (iii) and TiO_2 doped with 0.5 wt % Nd. (iv) A = anatase and R = rutile.

removed and centrifuged at 3500 for 5 min. The supernatant was separated and analyzed. The efficiency of the different catalysts was evaluated by monitoring RB decolorization, which indicates the dye degradation, and total organic carbon (TOC) reduction, which indicates the dye mineralization. The dye degradation was evaluated spectrophotometrically (Femto 700S Spectrophotometer, absorption maximum of $\lambda = 600$ nm). The mineralization was evaluated by total organic carbon measurements (Shimadzu 5000A analyzer).

Adsorption of the substrate onto the catalysts was examined by stirring 15 mg of the catalyst in 20 mL of the appropriate concentrations of the substrates (RB aqueous solution: 1, 2, 3, 4, 5, 10, 25×10^{-5} mol L^{-1}). After equilibration for 40 min, the catalyst was filtered and the concentration of the organic substrate was determined spectrophotometrically. The concentration of Remazol Black B before and after adsorption was measured.

3. Results and discussion

3.1. X-ray diffraction

The crystalline phase and the composition of TiO_2 and Nd–TiO_2 samples prepared using the sol–gel and precipitation methods were determined by X-ray powder diffractometry. XRD patterns of the different catalysts are shown in Fig. 1. XRD peaks at $2\theta = 25.3^\circ$ (1 0 1) and 48.0° in TiO_2 diffractograms are easily identified as the anatase crystalline form, whereas peaks at $2\theta = 27.9^\circ$ (1 1 0) and 55.1° are characteristic of the rutile crystalline form. XRD intensities of the anatase (1 0 1) peak and the rutile (1 1 0) peak were also analyzed. It can be noted that doped and undoped samples synthesized by the sol–gel method and calcinated at 580 °C have characteristic diffraction peaks assigned to the anatase and rutile phases. In pure TiO_2, rutile is the predominant phase with 74% in weight, while anatase represents 26%. However, in neodymium-doped samples the percentage of anatase is 64% and rutile is 36%.

The XRD patterns of Nd-doped and undoped TiO_2 synthesized by the precipitation method, both calcinated at 580 °C, are also shown in Fig. 1. The materials obtained by the precipitation method showed only diffraction peaks assigned to the anatase phase. It is interesting to note that the differences in crystalline phases of the catalysts arise from the type of synthesis route. In the catalysts prepared by precipitation, anatase predominates, while in TiO_2 doped or undoped obtained by sol–gel, a mixture of the anatase and rutile phases results. Parida and co-workers [26] synthesized TiO_2 doped with La^{3+}, Nd^{3+} and Pr^{3+} using the sol–gel method. The XRD patterns of lanthanide-doped TiO_2 (calcinated at 500 °C) are similar, containing only anatase; for pure TiO_2 calcinated at the same temperature, the predominant phase was rutile and anatase was found in a minor quantity. Xiao and co-workers [27] identified the same effect in Sm^{3+} doped TiO_2 with several samarium contents obtained by low temperature combustion synthesis (LCS). In undoped titania calcinated at 600 °C for 2 h, rutile is the dominant crystalline phase (97.5%), while Sm^{3+}-doped TiO_2 samples show a mixture of anatase and rutile, and the relative ratio of rutile to anatase is reduced with the increase of the samarium content. The inhibition of this phase transition was ascribed to the stabilization of the anatase phase by the surrounding lanthanide ions through the formation of anatase-O lanthanide bonds [28]. In the present case, possibly the formation and interaction of Nd–O–Ti takes place and inhibits the phase transition.

3.2. Thermal analysis

Fig. 2 shows TG curves of pure and Nd-doped TiO_2 obtained by both the sol–gel and precipitation methods. Materials synthesized by sol–gel exhibit a similar profile and the first decomposition step in the temperature range 25–100 °C corresponds to elimination of solvents. For this decomposition step, the weight loss was 9% and 11% for undoped and doped TiO_2, respectively. The weight loss of samples obtained by precipitation in the first decomposition step occurred between 32 and 190 °C and the weight loss was 18% for both pure and doped TiO_2. The second step of thermal decomposition of the materials prepared by the sol–gel method occurs in the temperature range of 100–400 °C. In the precipitation method the second thermal decomposition occurred between 190 and 400 °C, but for Nd-doped TiO_2 the mass loss occurs up to ca. 500 °C. The total weight losses measured from the TG curves were 31% and 24% for pure and Nd-doped TiO_2, respectively. The samples synthesized by sol–gel showed total weight losses of 19% for undoped TiO_2 and 22% for doped TiO_2.

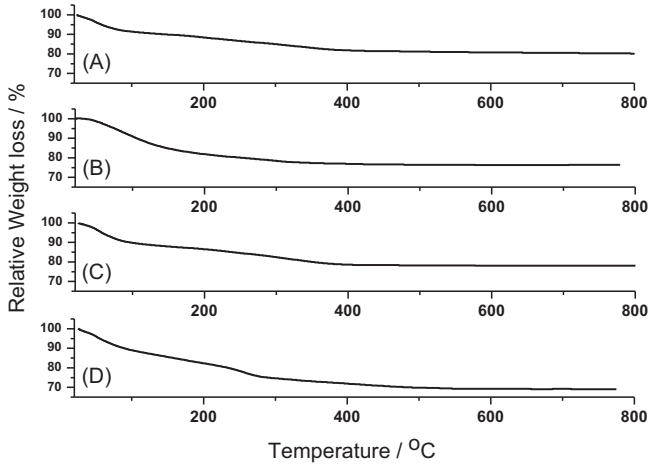

Fig. 2. TG curves of the undoped and doped TiO_2 synthesized by sol–gel: (A) pure TiO_2 and (C) TiO_2 doped with 0.5 wt% Nd, and precipitation: (B) pure TiO_2 and (D) TiO_2 doped with 0.5% Nd. All curves were obtained under dynamic air atmosphere (50 mL min^{-1}) and a heating rate of 10 °C min^{-1}.

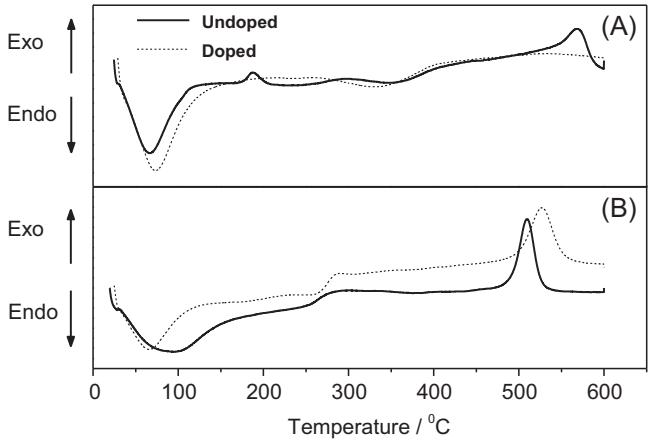

Fig. 3. DSC curves of the undoped and doped TiO_2 synthesized by sol–gel (A) and precipitation (B). All curves were obtained under dynamic nitrogen atmosphere (50 mL min^{-1}) and a heating rate of 10 °C min^{-1}.

DSC curves for photocatalysts synthesized using the sol–gel method are presented in Fig. 3(A). There is a distinct exothermic peak at 569 °C for undoped TiO_2. The exothermic peak in the range of 515–580 °C is attributed to the anatase to rutile transition, in agreement with X-ray patterns for this sample. The DSC curve of Nd-doped TiO_2 did not show any exothermic peak for temperatures higher than 400 °C. In this sample, anatase was the predominant phase, as observed in X-ray diffractograms. Due to neodymium ions present on the surface of doped TiO_2 particles the anatase to rutile phase transition was retarded. With the addition of neodymium ions to TiO_2, the exothermic peak in the DSC curve shifted to higher temperature (higher than 600 °C, not shown in DSC experiments). This effect is clearly visible in the samples synthesized using the precipitation method, Fig. 3(B). For undoped TiO_2, the exothermic peak related from the amorphous to anatase phase transition, occurred at 510 °C, but the presence of neodymium ions in TiO_2 shifted the transition peak to 527 °C.

Phase transition processes are quite complex in high surface area particulate materials and include several steps such as thermal degradation of tightly bound organic molecules, additional condensation of unhydrolyzed –OR groups, sintering and growth of particles and structural rearrangement of the newly formed Ti–O bonds [29,30]. In pure TiO_2, the experimental observation that the anatase to rutile phase transition initiates at the surface of bulk anatase is related to the high tangential diffusion of anatase nanospheres deduced by molecular dynamics simulations [31,32].

In general, ionic radius and calcination temperature are two of the most important parameters, which can strongly influence the ability of the dopant to enter into the TiO_2 lattice to form a stable solid solution. It can be seen in Fig. 1 that XRD peaks of pure and Nd-doped TiO_2 nanoparticles have the same positions and full width at half maximum, demonstrating that Nd^{3+} does not enter into the TiO_2 crystal lattice to substitute Ti^{4+}. This could be because the radius of Nd^{3+} (104 pm) is much bigger than Ti^{4+} (88 pm) [33]. In addition, the phase related to Nd could not be observed (Fig. 1), possibly because that Nd could be dispersed uniformly onto TiO_2 nanoparticles in the form of small agglomerated of Nd_2O_3. No crystalline phase of neodymium oxide was detected in Nd doped samples probably due to the very low doping content. Furthermore, Ti–O–Nd bonds around TiO_2 particles could occur during the process of thermal treatment, inhibiting the formation and growth of crystal nuclei, thereby retarding the phase transition. This effect was previously observed for other TiO_2 metal dopant [28,29].

Table 1 lists BET surface areas and particle sizes of the photocatalysts prepared in this study. The surface area and particle size of the samples was dependent on the preparation method and Nd presence. The surface area of the catalysts obtained by both synthesis is apparently increased when neodymium ions were present.

It is important to note that the surface area of Nd-doped samples synthesized by sol–gel and precipitation routes increased 14 and 1.5 times, respectively. As previously discussed, the neodymium could have an inhibitory effect on sintering and growth of TiO_2 particles. It is interesting to note the differences in the surface area and particle size of the undoped TiO_2 synthesized by the two routes. The BET area of TiO_2 obtained by the precipitation method was 81 $m^2 g^{-1}$ and by the sol–gel route 3.7 $m^2 g^{-1}$. This difference in the surface area was also observed for samples doped with neodymium. In general, the precipitation synthesis produced catalysts with larger surface area than the sol–gel method. The homogeneity of the neodymium dispersion with respect to TiO_2 crystal lattice, as well as the structural and photocatalytic properties of doped TiO_2, are dependent on the method of preparation. Thus, the differences in morphological and structural characteristics of all catalysts, i.e., surface area, temperature of the phase transition, crystallinity and the predominant crystal phase, are dependent on the method of preparation of pure and doped TiO_2. Furthermore, any comparison of the photocatalytic activity must take into account these individual characteristics of the catalysts.

3.3. Photocatalytic activities measurement

Fig. 4 shows the photocatalytic degradation of RB over the different TiO_2 catalysts under UV irradiation (<400 nm). By monitoring

Table 1
Surface area and particle size data for the undoped and doped TiO_2 synthesized by sol–gel and precipitation methods.

	Sol–gel		Precipitation	
	TiO_2	TiO_2–Nd	TiO_2	TiO_2–Nd
Surface area ($m^2 g^{-1}$)	3.7 ± 0.1	53.1 ± 1.1	81.0 ± 1.6	127.1 ± 2.5
Particle size (nm)	<100	29.4 ± 0.6	19.3 ± 0.4	12.3 ± 0.2

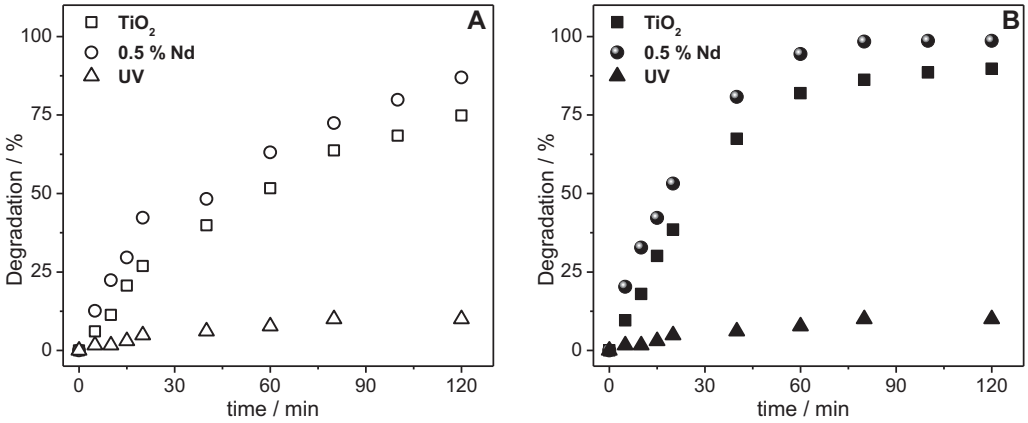

Fig. 4. Photocatalytic degradation curves of Remazol Black B on undoped and doped TiO_2 with 0.5 wt % neodymium ions synthesized by sol–gel (A) and precipitation (B).

the dye decolorization at 600 nm, it was possible to observe that the photochemical process using only UV irradiation allowed a dye degradation of just 10% even after 120 min of treatment. On the other hand, for the same treatment time, the photocatalytic process with TiO_2 reaches a degradation degree of 75% and 90% employing materials prepared by sol–gel and precipitation, respectively. The photocatalyst obtained by the precipitation method was more efficient probably due to the higher surface area and anatase content.

It is important to notice that the degradation of RB was higher for Nd-doped TiO_2 compared to undoped TiO_2, independently of the preparation route.

The influence of Nd was not only in the final values of RB decoloration (16% and 9% larger for sol–gel and precipitation, respectively), but also in the apparent first order rate constant (k) for the photocatalytic degradation. Comparing the materials obtained by precipitation, the rate constant for doped TiO_2 is around two times larger than undoped TiO_2 (Table 2). For photocatalysts obtained by sol–gel, the degradation processes using doped TiO_2 were faster than undoped TiO_2 and the rate constant was 37% larger.

These results showed that doping TiO_2 with neodymium really increases efficiency for degradation of Remazol Black. Besides TiO_2 surface changes (i.e. higher surface area), the complexation capacity of neodymium ions with Lewis base might be one of the reasons for this enhancement of the photocatalytic activity in the samples doped with this lanthanide. The maximum amount of RB adsorbed in the undoped TiO_2 was 2.2×10^{-6} mol $g_{catalyst}^{-1}$ and 3.0×10^{-6} mol $g_{catalyst}^{-1}$ for materials prepared by sol–gel and precipitation methods, respectively. On the other hand, for Nd–TiO_2 materials these values were 3.0×10^{-6} mol $g_{catalyst}^{-1}$ and 4.0×10^{-6} mol $g_{catalyst}^{-1}$. Indeed, the quantity of RB adsorbed at the surface of TiO_2 was higher for the doped catalysts.

The Nd dopant also can act as electron and/or hole traps. The trap of charge carriers can decrease the recombination rate of e^-/h^+ pairs and consequently increase the lifetime of charge carriers and the photocatalytic activity [17,34,35].

Table 2
Degradation and mineralization parameters showing the neodymium influence on the photocatalytic capacity of TiO_2 prepared by different methods after 120 min of treatment.

Photocatalyst	Decoloration (%)	k (h^{-1})	Mineralization (%)
TiO_2 (sol–gel)	74	0.69	29.1
TiO_2–Nd (sol–gel)	86	0.94	39.6
TiO_2 (precipitation)	89	1.42	52.7
TiO_2–Nd (precipitation)	98	3.07	57.7

The adsorption and photoactivity of the catalysts studied were independent of the pH in the range between 5.0 and 8.0, which is the most relevant range for natural water samples and many effluents.

Nevertheless, it is important to consider that the syntheses route and the presence of Nd(III) play a very important role in the allotropic phase titania constitution, the particle size and in the surface area. These are important parameters to define the photocatalytic activity of these materials.

4. Conclusion

The photoreactivities of undoped and Nd-doped TiO_2 prepared by sol–gel and precipitation routes were studied. Independent of the synthesis method, neodymium doping had an influence on the physical and chemical properties of TiO_2. XRD and thermal analyses indicated that neodymium ions change the transition phase temperature of TiO_2 and its surface area increased. Photocatalytic results for RB degradation showed that the photocatalytic efficiency of TiO_2 doped with only 0.5 wt % Nd is substantially enhanced compared to undoped TiO_2, independent of the synthetic method applied. The properties acquired by TiO_2 in the presence of neodymium increase the photocatalytic degradation efficiency of Remazol Black, an effect observed in catalysts synthesized by both methods.

Acknowledgements

The authors acknowledge the National Institute of Science and Technology for Environmental Studies (INCT-EMA), Brazilian Research Council (CNPq), State of São Paulo Research Foundation (FAPESP) and Center for Environmental Research and Training (CEPEMA-USP). The authors also thank Professor Paulo C. Isolani and Professor Frank Quina for the English revision. The authors are grateful to Professor Claudio A. Oller Nascimento coordinator of the Chemical Systems Engineering Center (CESQ/DEQ-EPUSP) and CEPEMA/USP for the analytical facilities.

References

[1] R.S. Freire, T.L. Kubota, N. Duran, Environ. Technol. 21 (6) (2000) 717–721.
[2] T. Oppenlander, Photochemical Purification of Water and Air, Wiley-VCH, 2003.
[3] 0. Legrini, E. Oliveros, A.M. Braun, Chem. Rev. 93 (2) (1993) 671–698.
[4] T.L. Thompson, J.T. Yates, Chem. Rev. 106 (10) (2006) 4428–4453.
[5] M.I. Litter, Appl. Catal. B 23 (2–3) (1999) 89–114.
[6] M.A. Fox, M. Dulay, Chem. Rev. 93 (1) (1993) 341–357.
[7] M.R. Hoffmann, S.T. Martin, W. Choi, D.W. Bahnemannt, Chem. Rev. 95 (1) (1995) 69–96.
[8] T. Docters, J.M. Chovelon, J.M. Herrmann, J.P. Deloume, Appl. Catal. B 50 (4) (2004) 219–226.

[9] S.K. Poznyak, A.I. Kokorin, A.I. Kulak, J. Electroanal. Chem. 442 (1–2) (1998) 99–105.
[10] F.B. Li, X.Z. Li, Appl. Catal. A 228 (1–2) (2002) 15–27.
[11] H. Dislich, J. Non-Cryst. Solids 80 (1986) 115–121.
[12] J. Livage, M. Henry, C. Sanchez, Prog. Solid State Chem. 18 (1988) 259–341.
[13] U.I. Gaya, A.H. Abdullah, J. Photochem. Photobiol. C 9 (1) (2008) 1–12.
[14] T. López, F. Rojas, R. Alexander-Katz, F. Galindo, A. Balankin, A. Buljan, J. Solid State Chem. 177 (2004) 1873–1885.
[15] T. Tachikawa, M. Fujitsuka, T. Majima, J. Phys. Chem. C 111 (14) (2007) 5259–5275.
[16] J. Liqiang, S. Xiaojun, X. Baifu, W. Baiqi, C. Weimin, F. Hongganga, J. Solid State Chem. 177 (10) (2004) 3375–3382.
[17] Y. Wang, H. Cheng, L. Zhang, Y. Hao, J. Ma, B. Xu, W. Li, J. Mol. Catal. A: Chem. 151 (2000) 205–216.
[18] Y. Xiea, C. Yuan, L. Xiangzhong, Colloids Surf. A 252 (1) (2005) 87–94.
[19] Y. Xie, C. Yuan, L. Xiangzhong, Mater. Sci. Eng. B 117 (3) (2005) 325–333.
[20] Y.H. Xu, C. Chen, X.L. Yang, X. Li, B.F. Wang, Appl. Surf. Sci. 255 (2009) 8624–8628.
[21] B. Shahmoradi, I.A. Ibrahin, N. Sakamoto, S. Ananda, R. Somashekar, T.N. Guru Row, K. Byrappa, J. Environ. Sci. Health A: Toxic/Hazard. Subst. Environ. Eng. 45 (2010) 1248–1255.
[22] C. Wang, Y. Ao, P. Wang, J. Hou, J. Qian, Appl. Surf. Sci. 257 (2010) 227–231.
[23] M.R. Mohammadi, D.J. Fray, A. Mohammadi, Micropor. Mesopor. Mater. 112 (1–3) (2008) 392–402.
[24] M. Vallet-Regi, J. Peña, A. Martinez, J.M. Gonzalez-Calbet, Solid State Ionics 63–65 (1993) 201–206.
[25] R.A. Spurr, H. Myers, Anal. Chem. 29 (5) (1957) 760–762.
[26] K.M. Parida, N. Sahu, J. Mol. Catal. A: Chem. 287 (1–2) (2008) 151–158.
[27] Q. Xiao, Z. Si, Z. Yu, G. Quiu, J. Alloys Compd. 450 (1–2) (2008) 426–431.
[28] J. Arbiol, J. Cerda, G. Dezanneau, A. Cirera, F. Peiro, A. Cornet, J.R. Morante, J. Appl. Phys. 92 (2) (2002) 853–861.
[29] J. Frenkel, J. Phys. 9 (5) (1945) 392.
[30] J.K. Mackenzie, R. Shuttleworth, Proc. Phys. Soc. 62 (12-B) (1949) 833–852.
[31] U. Diebold, Surf. Sci. Rep. 48 (2003) 53–229.
[32] S. Ogata, H. Iyetomi, K. Tsuruta, F. Shimojo, A. Nakano, K.R. Kalia, P. Vashishta, J. Appl. Phys. 88 (10) (2000) 6011–6015.
[33] J.C. Slater, J. Chem. Phys. 41 (1964) 3199–3204.
[34] S.I. Shah, W. Li, C.P. Huang, O. Jung, C. Ni, Proc. Natl. Acad. Sci. U.S.A. 99 (2) (2002) 6482–6486.
[35] W. Li, A.I. Frenkel, J.C. Woicik, C. Ni, S.I. Shah, Phys. Rev. B 72 (15) (2005) 155315–155317.